Am J Cancer Res 2022;12(1):198-209
www.ajcr.us /ISSN:2156-6976/ajcr0139608

Original Article

Enhanced proton treatment with a LDLR-ligand peptide-conjugated gold nanoparticles targeting the tumor microenvironment in an infiltrative brain tumor model

Seungjun Seo[1*], Eun Ho Kim[2*], Won-Seok Chang[1], Won-Seok Lee[2], Ki-Hwan Kim[3], Jong-Ki Kim[1]

[1]Biomedical Engineering and [2]Biochemistry, School of Medicine, Daegu Catholic University, Daegu, South Korea; [3]Radiation Oncology, College of Medicine, Chungnam National University, Daejeon, South Korea. [*]Equal contributors.

Received October 6, 2021; Accepted December 3, 2021; Epub January 15, 2022; Published January 30, 2022

Abstract: The tumor microenvironment (TME) of glioblastoma malforms (GBMs) contains tumor invasiveness factors, microvascular proliferation, migratory cancer stem cells and infiltrative tumor cells, which leads to tumor recurrence in the absence of effective drug delivery in a Blood Brain Barrier (BBB)-intact TME and radiological invisibility. Low-density lipoprotein receptor (LDLR) is abundant in the blood brain barrier and overexpressed in malignant glioma cells. This study aimed to treat the TME with transmitted proton sensitization of LDLR ligand-functionalized gold nanoparticles (ApoB@AuNPs) in an infiltrative F98 glioma rat model. BBB-crossing ApoB@AuNPs were selectively taken up in microvascular endothelial cells proliferation and pericyte invasion, which are therapeutic targets in the glioma TME. Proton sensitization treated the TME and bulk tumor volume with enhanced therapeutic efficacy by 67-75% compared to that with protons alone. Immunohistochemistry demonstrated efficient treatment of endothelial cell proliferation and migratory tumor cells of invasive microvessels in the TME with saving normal tissues. Taken together, these data indicate that the use of LDLR ligand-functionalized gold nanoparticles is a promising strategy to treat infiltrative malignant glioma while overcoming BBB crossing.

Keywords: Tumor microenvironment, proton stimulation, glioblastoma malforme, BBB crossing, LDLR-transcytosis, TME targeting gold nanoparticles

Introduction

Glioblastoma multiforme (GBM) presents diverse mechanisms of invasion that can be activated depending on the cell of origin (tumor cell or stem cell) in the tumor microenvironment [1]. Glioma stem cells contribute to the formation of tumor blood vessels by differentiating into endothelial cells or pericytes [2, 3], which results in microvascular proliferation (MVP) with hyperproliferation and the accumulation of endothelial cells around vessel lumens [3, 4]. MVP contributes to the rapid growth of glioblastoma [4]. GBM cells infiltrate the surrounding tissue via perivascular migration, which results in the formation of microscopic tumor extensions beyond the margins of surgical resection [5]. Therefore, both stem cell-driven angiogenesis, including endothelial cell proliferation and the perivascular migration of tumor cells in the tumor microenvironment, should be treated together to control glioblastoma invasion [1, 6]. Otherwise, they remain a source of tumor recurrence when untreated in an integrative way [7, 8]. A major hurdle in the clinical management of GBM invasiveness is intact BBB in the radiologically invisible invasive front of the tumor and normal cortex, which contain invaded glioblastoma cells, cancer stem cells (CSCs), pericytes and endothelial cell proliferation in MVP, thus leading to cancer cell treatment resistance [7, 9, 10]. To target the tumor microenvironment in glioblastoma, any drug delivery system must be desired to cross the intact BBB prior to entering tumor or cancer-origin proliferating cells. Nanometer-scale particles represent one

class of agents that could better extravasate into brain tumor tissue given a more permeable BBB, and they may represent a promising candidate for permeability across the BBB [11-13].

Low-density lipoprotein receptor (LDLR) has been reported to be highly expressed on the BBB and glioma cells [14, 15] and has been used as a BBB crossing platform [16]. All results have indicated that LDLR is a potential molecular target for the selective delivery of antitumor agents to glioma [17].

The ApoB29 mer peptide is the binding domain of a ligand of LDLR [18-20], and ApoB-conjugated gold nanoparticles are potentially BBB-crossing radiosensitizers for targeting infiltrative MVP and promoting perivascular invasion in GBM. Proton treatment is known to induce apoptosis of CSCs more effectively through ROS generation than conventional X-ray photon radiotherapy [21]. Moreover, proton-stimulated high-Z nanoparticles produce ROS in a tissue-oxygen independent manner [22], potentially curing the hypoxic environment and CSCs in glioblastoma. In this study, we investigated the tumor microenvironment, including tumor infiltration and endothelial cell proliferation of MVP, with proton-stimulated radiosensitization of ApoB peptide-conjugated gold nanoparticles dual-targeting the BBB and glioma in an infiltrative brain tumor model.

Materials and methods

Synthesis and characterization of ApoB-conjugated gold nanoparticles

ApoB@AuNPs or ApoB@AuNPs-Cy5s were synthesized by thiolating the ApoB peptide (3-mercaptopropionic acid-DWLKAFYDKVAEKLKEAFRLTRKRGLKLA-NH2: Anygen, Korea) or SH-PEG5000-Cy5.5 (Intechim, France) together with peptide to 15-nm gold NPs (Nanoprobe, USA) using the same method described previously [23]. Excessive 500 μM ApoB peptide dissolved in 1 mL of DMSO was mixed with 100 μM 15 nm AuNPs. For the synthesis of ApoB1@AuNP-Cy5.5, one-milliliter stock solutions of AuNPs (0.5 mg/mL, 2.538 mM), SH-PEG-Cy5.5 (1 mM) in distilled water, and ApoB peptide (2.863 mM) in dimethyl sulfoxide (DMSO) were prepared. In a typical synthesis of 10 μM ApoB@AuNP-Cy5.5 nanocomplexes, Then, 928.56 μL of distilled water was added to a bottle prior to mixing with 50 μL of SH-PEG-Cy5.5 and 17.5 μL of 100 μM ApoB peptide for 5 min while stirring to produce a 1:1 molar ratio of SH-PEG-Cy5.5 to ApoB peptide. Then, 3.94 μL of AuNP solution was added to the mixture of SH-PEG-Cy5.5/ApoB peptide, which results in a 5:1 molar ratio of thiol to gold at pH 7.4. Finally, the mixture of SH-PEG-Cy5.5/ApoB/AuNPs was stirred at room temperature for 2 h to allow for the complete formation of gold nanocomplexes. Reactions were performed by shaking the mixture for two hours, and gold nanoparticles were precipitated by centrifugation for 10 min. After decanting the supernatant, the pellet was resuspended in 0.5 or 1 mL of phosphate-buffered saline (PBS).

Functionalized nanocomplexes with HCy5.5 (ApoB@AuNP-HCy5) were prepared as previously reported [24]. Briefly, ApoB@AuNP-Cy5.5 was dissolved in 1 mL of methanol to generate a 50-μM solution and placed in a sealed vial. Sodium borohydride (NaBH4, 20 μM) was added to this nanocomplex solution, which was subsequently mixed by stirring for 10 min at room temperature. Unreacted sodium borohydride molecules were removed by centrifugation at 16,000 rpm for 10 min. After decanting the supernatant, the pellet was resuspended in methanol.

ROS measurement of ApoB@AuNP-HCy5

Proton impact measurements were performed on a series of water phantoms containing hydrocyanine-nanocomplex solution using a 100 MeV proton transmission beam at the Korea Multi-Purpose Accelerator Complex (Gyeongju, Korea).

ROS (i.e., either $^{\cdot}OH$ or O_2^{-}) were measured in situ using the ROS oxidant HCy5.5 in ApoB@AuNP-HCy5.5 under proton irradiation as previously described [22]. Hydrocyanine-nanocomplex solutions containing varying concentrations of ApoB@AuNP-HCy5.5 (0, 0.2, or 20 μM) were irradiated by a proton transmission beam with two different plateau doses (0, 2, or 4 Gy). Three batches of samples in each experimental group were treated with each radiation dose for each concentration of hydrocyanine-nanocomplex solution. The fluorescence signal of the oxidant (ApoB@AuNP-Cy5.5) after reacting with either superoxide or hydroxyl radicals was measured using a fluorescence microplate reader (Infinite, TECAN, Männedorf, Switzerland) immediately after irradiation. The average values

of the measured fluorescence signals from three wells per dose were plotted as a function of the proton irradiation dose.

Cell culture

Primary cultures of human brain microvascular endothelial cells (HBMECs; catalog no. 1000) and human astrocytes (HAs; catalog no. 1800) were purchased from ScienCell Laboratories (Carlsbad, CA) and cultured according to the supplier's instructions. Primary HBMECs and HAs were obtained at passage 2 and used for all experiments between passages 2 and 8.

TEER measurement and cellular uptake for BBB crossing of ApoB@AuNPs

The electrical resistance of a cellular monolayer, measured in ohms, is a quantitative measure of barrier integrity. The BBB model was established according to a previously described procedure [25]. The model consisted of two-compartment wells in a culture plate with the upper compartment separated from the lower compartment by a cyclopore polyethylene terephthalate membrane (Collaborative Biochemical Products, Becton Dickinson, San Jose, CA) with a pore diameter of 3 mm. In a 24-well cell culture insert, 2.5×10^5 primary HBMECs were grown to confluency on the upper side, whereas a confluent layer of primary HAs (2.5×10^5 cells/insert) was grown on the underside. The intact BBB was determined by measuring the transendothelial electrical resistance (TEER) using Millicell ERS microelectrodes (Millipore, Billerica, MA). The electrical resistance of blank inserts with medium alone was subtracted from TEER readings obtained from inserts with confluent monolayers [26]. The resulting TEER values represent the resistance of the endothelial cell monolayers. The BBB model was used for experiments at least 5 days after cell seeding. The BBB constructs were treated with variable concentrations (10, 20, 50 μM) of either bare AuNPs or ApoB@AuNPs. TEER measurements were performed at 12 and 24 h after the treatment. The absorbance of the media after crossing the in vitro BBB model was measured. The typical TEER values for untreated cultures were 140~150 ohms/cm^2 [26]. Baseline values were absorbance per 1 mL of medium containing variable concentrations (10, 20, 50 μM) of gold nanoparticles, which was assumed to have 100% transmission. The amount of nanoparticles that was taken up in the cells was measured with inductively coupled plasma mass spectrometry (ICP-MS; Thermo Jarrell Ash ARISAP).

Orthotopic F98 glioma rat model and MRI imaging

All animal experiments were approved by the Institutional Animal Care and Use Committee at Daegu Catholic University Medical Center (DCIAFCR-171020-13Y). A total of 2×10^5 F98 glioma cells were implanted in the frontal lobe of Fischer 333 rats by stereotactic surgery as described previously [20]. Briefly, after immobilizing the rats in a rodent stereotactic frame, an incision was made in the skin, and a burr hole was made in the skull. One million tumor cells were injected at a rate of 1-2 microliters/minute using a microsyringe (Hamilton, Reno, NV, US) mounted on a stereotactic frame (Kopf Instruments, Tujunga, CA, US) at coordinates of 1 mm lateral and 1 mm posterior to the bregma and 1.5 mm below the dura. Tumor growth was evaluated with 4.7 T MRI 5 days after implanting the cells. In this study, a total of 12 rats were divided into three experimental groups for two irradiation doses (10 and 5 Gy), and three rats were left untreated to act as a control.

Uptake study of ApoB@AuNP-Cy5.5 in the tumor microenvironment and tumor mass

Either ApoB@AuNP-Cy5 (150 mg/BW, 75 mg/BW) or bare AuNP-Cy5 (150 mg/BW, 75 mg/BW) was injected into each glioma model, and the brain was extracted 24 hours postinjection of nanoparticles after sacrifice with contusion. The brain was divided into two parts, and fluorescence imaging of the haploid glioma brain was performed with an in vivo fluorescence imaging system (FOBI, NeoScience Co. Ltd., Korea), where gold nanoparticles were taken up by demonstrating a large enhancement of tumor uptake by BBB-crossing and glioma LDLR-targeting gold nanoparticles.

Proton treatment and analysis

A pristine proton beam was irradiated in three port directions with a Bragg peak inside the tumor mass in a rat glioma model at the Korea Multi-Purpose Accelerator Complex (Gyeongju, Korea), as shown in **Figure 1**. The depth of the

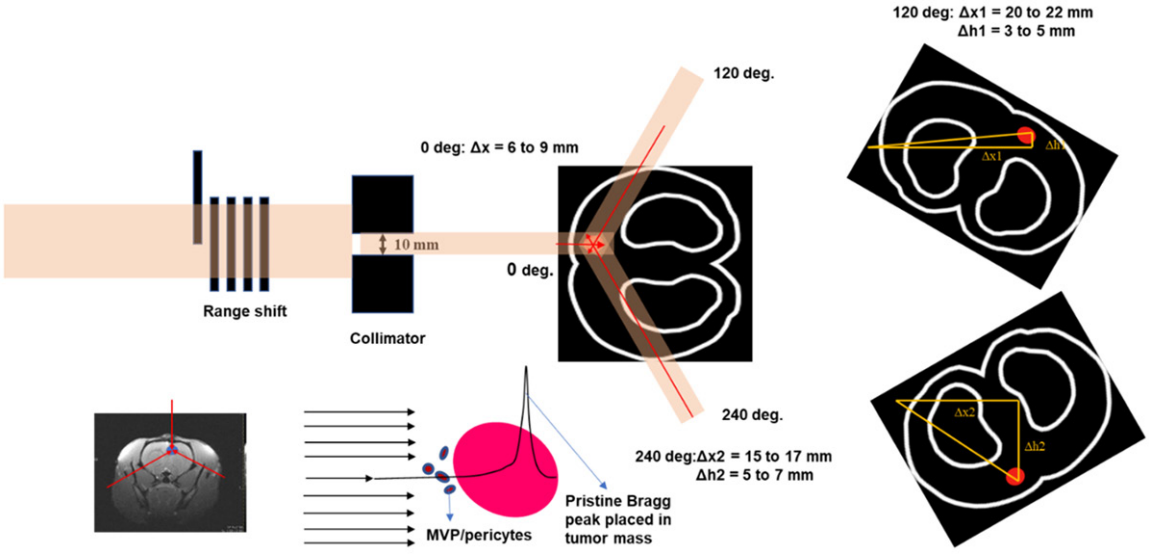

Figure 1. Schematic diagram of pristine proton irradiation in the three ports direction, placing the Bragg peak inside the tumor volume to treat the TME via transmitted protons while controlling the tumor volume with the Bragg peak dose. Tumor depth from the brain surface was adjusted in each direction to place the Bragg peak precisely inside the tumor volume.

tumor (Δx) and vertical deviation (Δh) from the surface of the mouse brain after rotation of the mouse were estimated with respect to the fixed proton beam direction based on MRI imaging, and the actual BP position was calculated as $\sqrt{(\Delta x^2 + \Delta h^2)}$. Accordingly, range shifts were adjusted to place the BP in the tumor mass according to the calculated depth of the BP in each direction of irradiation. The pristine proton beam was irradiated with an entrance dose of 4 Gy in each direction. Dosimetry at the actual sample position and the BP energy outside the sample were determined by measuring the radiation dose with a pair of range shifters and sandwiched radiochromic films (MD-V3 and HD-V2, Ashland Inc., Covington, KY) of 1-mm intervals and read with a scanner (Epson Perfection V700 Photo, Ashland Inc., Covington, KY). The entrance dose was measured just in front of the sample tube, and the plateau dose was measured at three different positions inside the sample. Both entrance and plateau dose were same scale. The BP was typically determined at 76 mm for 100 MeV from the frontal surface of the sample tube. The resulting entrance dose rate was 0.51 Gy/s. The irradiation period was controlled to generate entrance doses of 4 Gy. Tumors of mice were imaged with MRI before and after proton irradiation to measure the change in tumor volume and sacrificed 5 days post proton irradiation. Counting MVP with ECH or migratory perivascular tumor cells was performed on H&E-stained tissue sections (10 sections per mouse).

Immunofluorescence analysis

Tissues were fixed in 10% (v/v) neutral-buffered formalin, embedded in paraffin (FFPE), and sectioned. The sections were then deparaffinized and stained. Immunofluorescence staining was performed in antigen retrieval citrate buffer (Sigma; #C9999) at 95°C for 30 min. Next, the cells were permeabilized for 15 min with PBS containing 0.1% Triton X-100 (PBST) and blocked for 30 min with PBST containing normal horse serum. Next, the primary antibody was reacted, and the primary antibodies used were CD31 (Endothelial cell marker; 1:200; R&D Systems; #AF3628), αSMA (Fibroblast marker; 1:1000; Sigma-Aldrich; #A5228), Ki67 (Proliferation marker; 1:200; Acris, #DRM004) and VEGF (1:100; Santa-cruz, #SC-57496). For immunofluorescence, a secondary fluorescent antibody was used, and the nuclei were stained with DAPI (Sigma; #D9542).

Results

Synthesis of ApoB@AuNPs and ApoB@AuNP-Cy5s

The conjugation of ApoB29mer or SH-PEG-5000-Cy5 to 15-nm gold NPs shifted the opti-

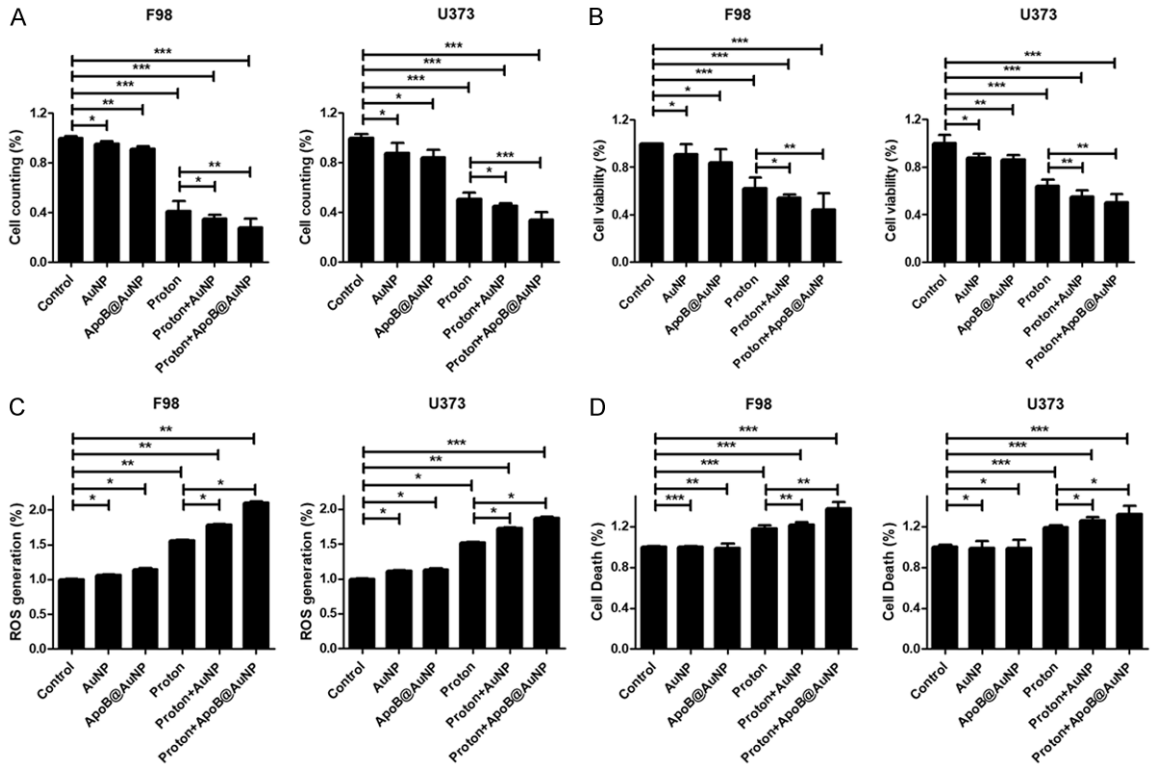

Figure 2. Radiosensitivity and ROS production in glioma cells treated in various ways. (A, B) F98 and U373 cells were exposed to proton beam for 48 h and/or pretreated bare AuNPs or ApoB@AuNPs 24 h prior to radiation for cell counting (A), the MTT assay (B). *P<0.05, **P<0.01, ***P<0.001. (C) Analysis of ROS generation in F98 and U373 cell lines 72 h after treatment with the indicated treatment by a ROS detection kit. *P<0.05, **P<0.01, ***P<0.001. (D) Analysis of cell death in F98 and U373 cell lines 72 h after treatment with the indicated treatment using a cell death detection kit. *P<0.05, **P<0.01, ***P<0.001. The highest sensitivity and ROS production were observed in ApoB@AuNP-treated glioma cells.

cal absorption of AuNPs, thereby indicating the formation of thiolating bonds (see Supplementary Figure 1). In the case of ApoB@AuNP-Cy5, red fluorescence was detected without quenching due to the presence of PEG linking.

Combined effects of ApoB@AuNP and protons on the radiosensitivity of glioblastoma tumor cell lines

To evaluate the radiosensitive effects of ApoB@AuNPs on proton-induced cytotoxicity, we performed trypan blue and MTT cell viability tests on GBM cell lines. The mixture of the proton beam and ApoB@AuNP therapy had a considerably higher anticancer impact on F98 and U373 cells than that of the individual treatment or bare AuNP plus proton combination (**Figure 2A**, **2B**). To ascertain the relationship between the production of reactive oxygen species (ROS) and the enhancement of ApoB@AuNPs and proton-induced apoptosis, we examined the effects of the proton-irradiated ApoB@AuNP-HCy5.5 combination on ROS production in vitro. ApoB@AuNP and proton radiation therapy enhanced the formation of ROS in GBM cancer cells (**Figure 2C**, **2D**), thereby indicating that ROS produced by the ApoB@AuNP and proton beam treatment boosted intracellular GBM cell death. In addition, the effect of protons was more pronounced with ApoB@AuNPs than with bare AuNPs.

ApoB@AuNP cross BBB model

ApoB-conjugated nanoparticles crossed a transmembrane BBB model in a dose-dependent manner, as shown in **Figure 3** and **Table 1**. The relative ratio of BBB-crossing ApoB@AuNPs to bare AuNPs increased with nanoparticle dose, reaching approximately 20 at 50 μM, suggesting LDLR-mediated transcytosis via LDLR-binding ApoB29 peptide ligand.

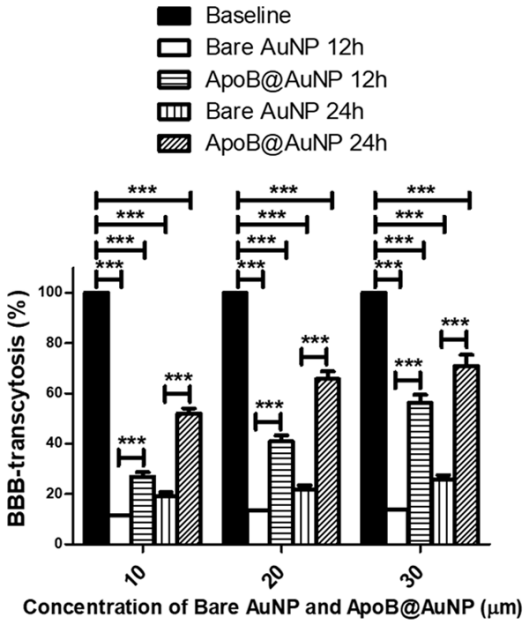

Figure 3. Traversing of various molecular groups over the BBB model. LDLR-targeting ApoB@AuNPs showed enhanced transmittance compared with bare gold NPs in a dose-dependent manner. Baseline is a measured optical absorption of ApoB@AuNP that was assumed as transmitted through the membrane entirely for a given amounts of applied nanoparticles.

Table 1. Concentration of nanoparticles taken up in astrocyte transmembrane of model BBB

Nanoparticles	10 μM	20 μM	50 μM
Bare AuNP	0.502	0.789	1.084
ApoB@AuNP	5.358	14.094	22.629

ROS generation of proton irradiated ApoB@AuNP-HCy5.5

Electrons and X-ray fluorescence emitted from proton-irradiated gold nanoparticles produced ROS in aqueous solution, which was measured in situ in the vicinity of nanoparticles via fluorescence from the ROS-mediated reoxidation of a hydrocyanine compound. ROS-driven fluorescence increased with proton dose at two different concentrations of gold nanoparticles, as shown in **Figure 4**.

Enhanced uptake of ApoB@AuNP-Cy5.5 in the tumor microenvironment and tumor mass

Either ApoB@AuNP-Cy5 (150 mg/BW, 75 mg/BW) or bare AuNP-Cy5 (150 mg/BW, 75 mg/

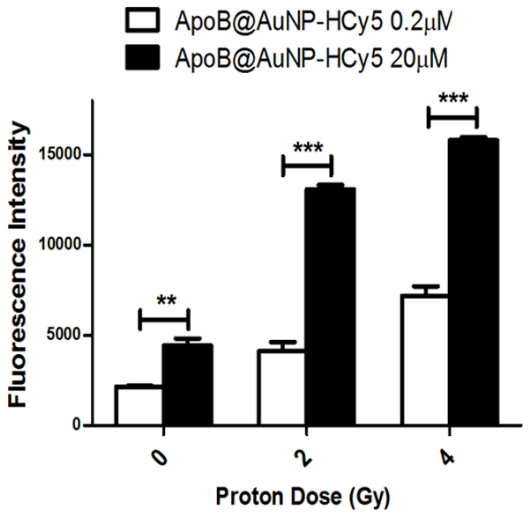

Figure 4. In situ measurements of ROS production from proton-sensitized gold nanoparticles. Recovered fluorescence was measured upon oxidized cyanine by ROS-reacted nonfluorescent hydrocyanine.

BW) was injected into each glioma model, and the brain was extracted 24 hours postinjection of nanoparticles after sacrifice with contusion. The brain was divided into two parts, and fluorescence imaging of the haploid glioma brain was performed with an in vivo fluorescence imaging system (BioFL, Korea), where gold nanoparticles were taken up by demonstrating large enhancement of tumor uptake by BBB crossing and glioma LDLR-targeting gold nanoparticles, as shown in **Figure 5**.

Red fluorescence of ApoB@AuNP-Cy5 was detected dose-dependently in MVP or the perivascular region surrounding the tumor mass, as shown in **Figure 5**, thereby indicating the uptake of nanoparticles in endothelial cell proliferation or the perivascular migration of tumor cells in the TME. To the best of our knowledge, this uptake of gold nanoparticles in the neoplastic TME of an infiltrative brain tumor model was reported for the first time, suggesting a unique opportunity for either proton stimulation or efficient drug delivery in the TME.

Enhanced therapeutic effect on tumor mass and TME from proton-sensitized gold NPs

Tumor volumes of all experimental groups were imaged by MRI and measured before and after treatment longitudinally. Single proton treatment with a relatively low dose demonstrated growth retardation even in nanoparticle-sensi-

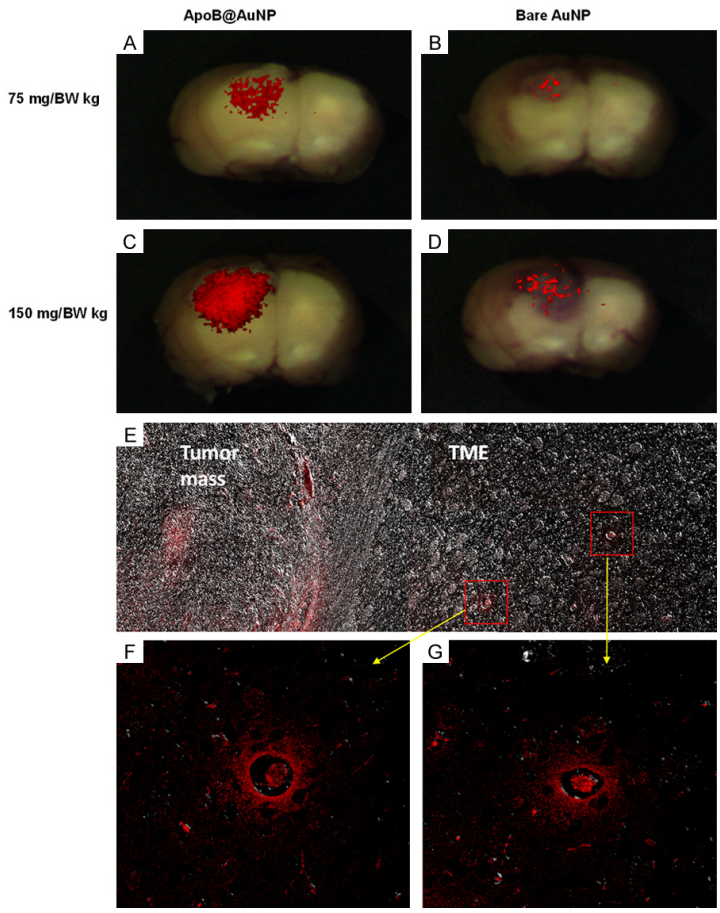

Figure 5. Fluorescence imaging of ex vivo brain haploids in which ApoB@AuNP (A, C) or bare gold NPs (B, D) were given intravenously prior to sacrifice and extraction. Observation of the red fluorescence of ApoB@AuNP-Cy5 in endothelial cell proliferation or perivascular tumor cell migration in the TME at 24 hours post intravenous injection of NPs (E). (F, G) Expanded view of (E) showed distribution of NPs-uptake at the neoplastic sites of TME more clearly.

tized treatment. Combined proton treatment with ApoB@AuNPs showed a 67% greater reduction in tumor volume than proton-alone therapy, as shown in **Figure 6**. Infiltrated angiogenic tumor invasion in 4 Gy combined treatment was greatly reduced by 75% more than ($P<0.001$) that with protons alone, as shown in **Figure 7B**. Moreover, the number of MVP-like structures without endothelial cell proliferation or cancerous cells in combined therapy was more than double compared with that obtained with protons alone, as indicated in **Figure 7C**. In contrast, the untreated control and protons alone showed a large amount of pseudopalisade and intact endothelial cell hypertrophy of MVP in the TME, respectively, as shown in **Figure 7A**.

In the case of single proton stimulation with a 10-Gy pristine transmission beam, this therapeutic effect on the TME was also evident (see Supplementary Figure 2), which also presents the control of the tumor mass.

Immunofluorescence data showing enhanced reduction of the neoplastic TME by combined proton treatment with TME-targeted gold NPs

IF data showed the presence of the neoplastic nature of the TME, such as microvascular proliferation with endothelial cell hypertrophy and perivascular tumor cell migration in the untreated control group and a marked reduction in combined proton treatment, as shown in **Figure 8**. Endothelial cell proliferation with CD31+ was also accompanied by SMA+, representing vascular sprouting from pericytes for perivascular invasion that were surrounded by neoplastic Ki67+ in the untreated control. These appearances were notably reduced in either the central tumor mass or TME in nanoparticle-sensitized proton treatment. Endothelial cell proliferation remained with protons alone, as shown in the expanded window in **Figure 8A**, but not with NP-sensitized proton treatment.

Discussion

Endothelial cell hyperproliferation (ECH) in MVP [4, 27, 28] and perivascular migration of tumor cells as vessel co-options [5], which are characteristic vascular pathophysiologies in glioblastoma, lead to tumor invasion in the TME with both neoangiogenesis and sprouting angiogenesis [29]. The distribution of ApoB@AuNP-Cy5 in both the main tumor mass and BBB-intact TME showed its capability of BBB crossing and LDLR-based targeting to tumor tissue. Direct observations of BBB crossing and preferential uptake in endothelial cell proliferation or pericytes of ApoB@AuNPs in the target TME struc-

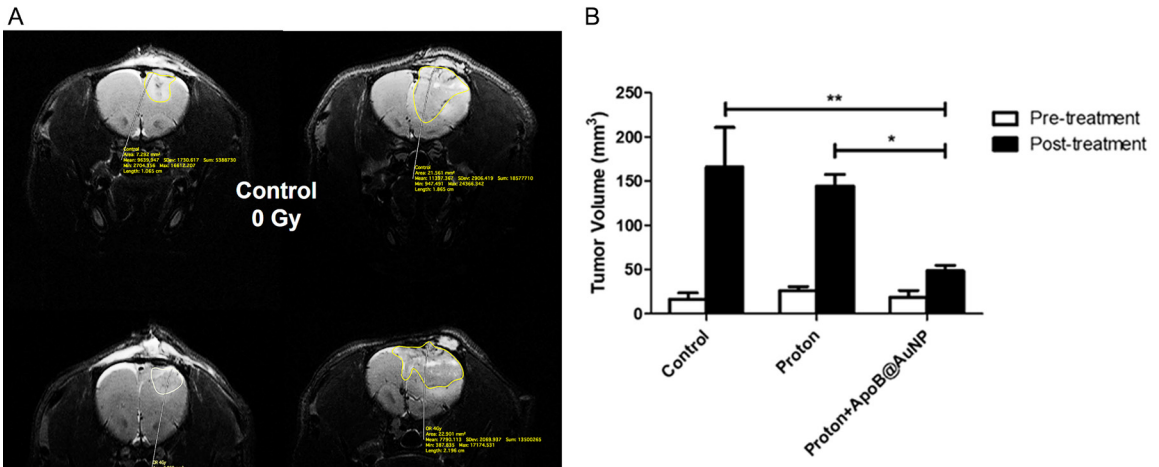

Figure 6. Tumor volumes of all experimental rat groups were measured by longitudinal MRI imaging. Proton-sensitized treatment showed a controlled tumor volume with a 67% relative reduction compared to that with protons alone.

ture are important for designing potential inhibitors for tumor invasion in GBM under the present status of incapable current antiangiogenic drugs [29]. The largest enhancement in radiosensitivity was also ascribed to preferential accumulation of ApoB@AuNPs in glioma cells in vitro and was evident from enhanced ROS production from proton irradiation of LDLR-targeted gold NPs. Endothelial cellular or pericyte uptake of ApoB@AuNPs may be ascribed to the nature of cancer stem cell-derived ECH or pericytes [7, 28, 30, 31], thus providing a unique therapeutic opportunity for both the neoplastic TME and tumor mass of GBM with proton stimulation to derive the Coulomb nanoradiator effect (CNR) [22, 32] from high-Z nanoparticles. In this work, a single treatment was performed by a pristine proton beam with an entrance dose corresponding to a similar scale of fractionated dose in conventional radiotherapy to stimulate ApoB@AuNP in TME without damaging normal tissue. The consequence of this effect resulted in the net growth of tumor volume in a single treatment compared with initial volume at pre-treatment. However, notable reduction of neoplastic TME structure and tumor volume with 4-Gy single proton-sensitized treatment compared with protons alone suggest a better outcome in control of either TME or tumor mass with repeated fractionation therapy in actual clinical setting. ECH remained in protons alone with 4 Gy, which was a similar dose of conventional fractionated radiotherapy, including proton treatment, which suggested inefficiency to remove the TME with conventional radiotherapy. The proton-sensitized dose not only enhanced the dose but also included CNR X-ray fluorescence-derived water radiolysis [22], which produces exogenous ROS in an oxygen-independent manner, which results in beneficial curing of tumor hypoxia in the TME and main mass via the potential formation of lipid peroxidation. Blocking neoangiogenic potential in both the tumor mass and TME, as shown by immunofluorescence analysis, may induce such therapeutic effects.

The main goal of this treatment was to control the TME by delivering high-Z nanoparticles and inducing CNR electron/X-ray fluorescence

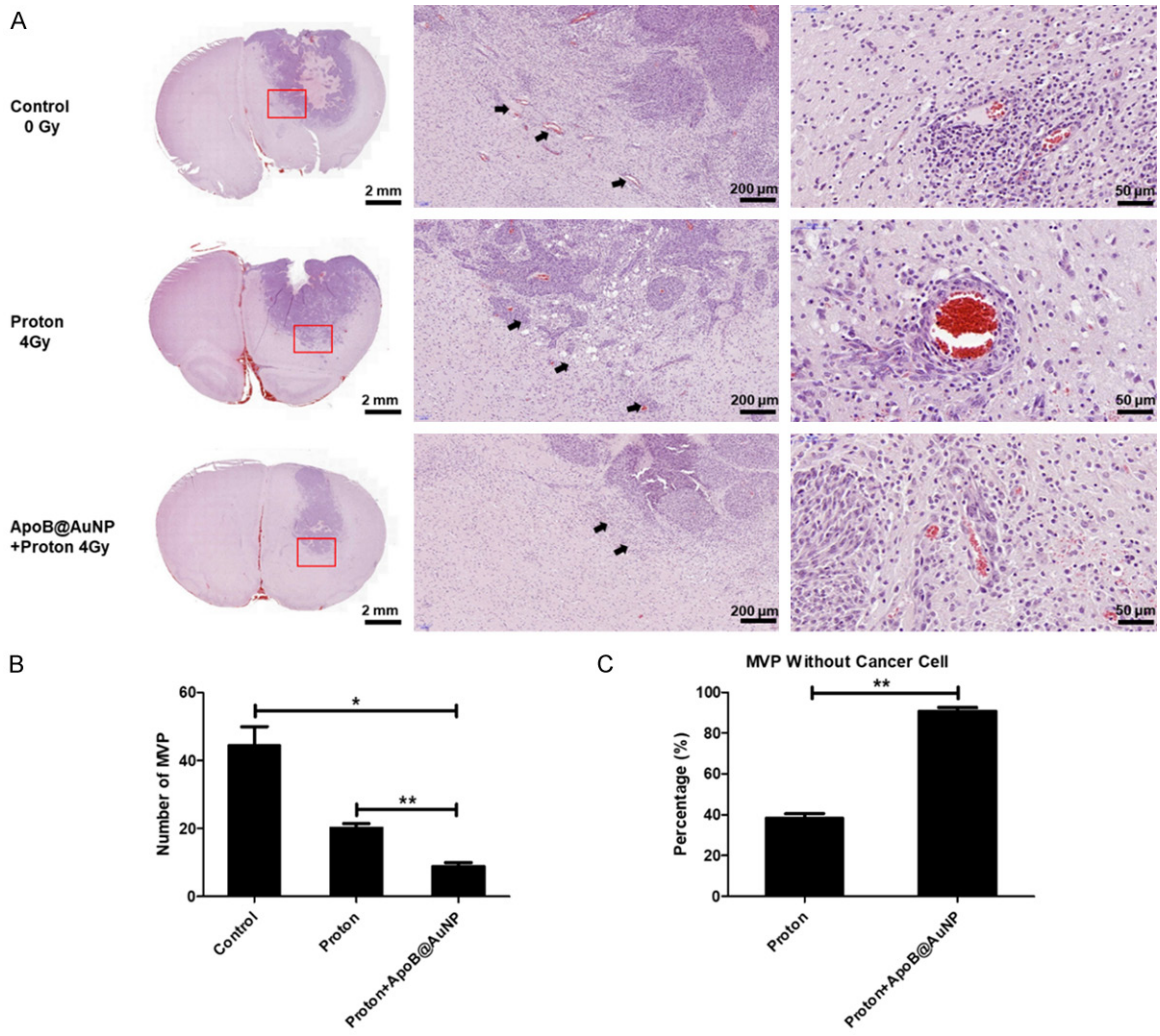

Figure 7. Histology (A) and counting (B, C) of neoplastic angiogenic tumor invasion in various experimental groups showed a relatively large reduction in microvascular proliferation or perivascular tumor cell migration in the combined treatment group where endothelial cell proliferation or pericyte tumor cells were absent compared to that with protons alone and the untreated control group.

emission [22, 32] in transmission proton mode, which was achieved by irradiating a pristine proton beam in the three ports direction, as shown in **Figure 1**. Proton fluence comparable to the Bragg peak dose traversed the TME region with tissue deposition at a value as much as 4 Gy of the plateau dose in the TME region and depositing 20 Gy of Bragg peak in tumor volume as previously described in detail [20]. Therefore, many protons, comparable to the Bragg peak dose, selectively interacted with high-Z gold NPs, thus producing a therapeutic effect on the NP-given TME structure while depositing a relatively small plateau dose in the TME; therefore, normal tissue was saved. This principle resulted in a much greater reduction in either tumor volume or TME structure with nanoparticle-sensitized proton treatment than with protons alone. Moreover, incidental placing of Bragg peaks in the radiologically occult TME often occurs due to elevated proximal entrance doses from SOBP and the resulting imprecise dose conformality near the penumbra may damage the normal tissue with incomplete therapeutic effects on the TME. In contrast, selective dose enhancement at the nanoparticle site provides better precision to localize the therapeutic dose only in the neoplastic structure of the TME without damaging the normal tissue.

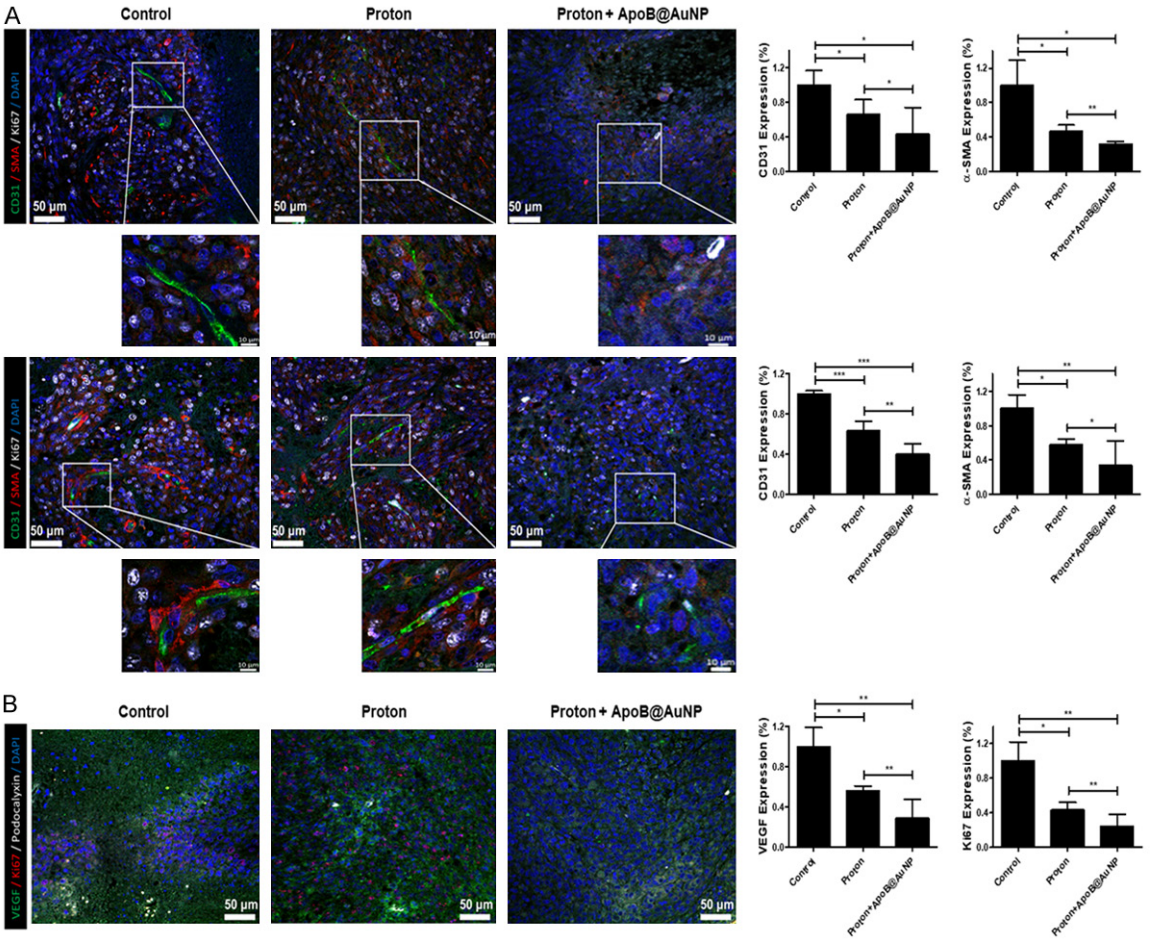

Figure 8. Immunofluorescence data (staining with CD31, SMA, Ki67, and VEGF) showing enhanced reduction of both tumor mass and neoplastic TME with angiogenic invasion such as endothelial cell proliferation and pericytes invasion by combined proton treatment with TME-targeted gold NP. (A) Immunofluorescence staining of CD31 (green) and αSMA (red) cells from control mice, proton treated or proton + ApoB@AuNP treated mice. (A, upper: tumor mass, A, lower: neoplastic TME with angiogenic invasion), Scale bar =50 μm. Quantification of an average of five fields with high appear $CD31^+$ αSMA^+ cells per field (magnification, 200×, n>5). For graphs, error bars indicate ± SD. $^*P<0.05$, $^{**}P<0.01$, $^{***}P<0.001$. (B) Immunofluorescence staining of VEGF (green) and Ki67 (red) cells from control mice, proton treated or proton + ApoB@AuNP treated mice. (A, upper: tumor mass, A, lower: neoplastic TME with angiogenic invasion), Scale bar =50 μm. Quantification of an average of five fields with high appear $VEGF^+$ $Ki67^+$ cells per field (magnification, 200×, n>5). For graphs, error bars indicate ± SD. $^*P<0.05$, $^{**}P<0.01$, $^{***}P<0.001$.

The large difference in BBB crossing and glioma uptake between ApoB29@AuNPs and bare AuNPs suggested the role of ApoB29 peptide-LDLR binding-mediated transcytosis in preferential transport or uptake. The tissue uptake of ApoB@AuNPs in ECH or pericytes suggested the potential expression of either LDLR or LDLR-related protein [33, 34] due to glioma stem cell-derived origin of these invasive vascular tissues. Therefore, immunofluorescence data showing a remarkable reduction in the proliferation of migratory tumor cells and cancer cell-origin microvascular cells from the treatment with LDLR-targeting gold nanoparticles indicated the neoplastic nature of the TME with presence of LDLR-like proteins. This finding is also helpful for designing new BBB-crossing antiangiogenic drugs that may in turn enable another combined therapy of GBM with antiangiogenic drugs and proton sensitization of tumor infiltration structures.

Collectively, proton-sensitized gold nanoparticles in the TME structure efficiently cure the neoplastic TME.

Conclusion

LDLR-ligand peptide-conjugated gold nanoparticles crossed the BBB and showed preferential uptake by microvascular endothelial cell proliferation and pericyte invasion of the TME. Proton-sensitized treatment with ApoB@AuNPs markedly reduced the neoplastic TME and tumor volume compared to that with protons alone.

Acknowledgements

This work was performed with financial support from the Radiation Technology Development (2015M2A2A7A01045270) through the National Research Foundation of Korea and partially from the Rare Isotope Science Project of the Institute for Basic Science funded by the Ministry of Science and ICT and NRF of Korea (2013M7A1A1075764).

Disclosure of conflict of interest

None.

Address correspondence to: Jong-Ki Kim, Biomedical Engineering and Radiology, Daegu Catholic University, School of Medicine, 33 Dooryugongwonro-17gil, Daegu, South Korea. Tel: +82-10-9685-4335; E-mail: jkkim@cu.ac.kr

References

[1] Rajapakse VN, Herrada S and Lavi O. Phenotype stability under dynamic brain-tumor environment stimuli maps glioblastoma progression in patients. Sci Adv 2020; 6: eaaz4125.

[2] Tena-Suck M, Celis-Lopez M, Collado-Ortiz M, Castillejos-Lopez M and Tenorio-Serralta M. Glioblastoma multiforme and angiogenesis: a clinicopathological and immunohistochemistry approach. Journal of Neurology Research 2015; 5: 199-206.

[3] Ricci-Vitiani L, Pallini R, Biffoni M, Todaro M, Invernici G, Cenci T, Maira G, Parati EA, Stassi G, Larocca LM and De Maria R. Tumour vascularization via endothelial differentiation of glioblastoma stem-like cells. Nature 2010; 468: 824-828.

[4] Kawasoe T, Takeshima H, Yamashita S, Mizuguchi S, Fukushima T, Yokogami K and Yamasaki K. Detection of p53 mutations in proliferating vascular cells in glioblastoma multiforme. J Neurosurg 2015; 122: 317-323.

[5] Seano G and Jain RK. Vessel co-option in glioblastoma: emerging insights and opportunities. Angiogenesis 2020; 23: 9-16.

[6] Norton KA and Popel AS. Effects of endothelial cell proliferation and migration rates in a computational model of sprouting angiogenesis. Sci Rep 2016; 6: 36992.

[7] Hambardzumyan D and Bergers G. Glioblastoma: defining tumor niches. Trends Cancer 2015; 1: 252-265.

[8] Stupp R, Mason WP, van den Bent MJ, Weller M, Fisher B, Taphoorn MJ, Belanger K, Brandes AA, Marosi C, Bogdahn U, Curschmann J, Janzer RC, Ludwin SK, Gorlia T, Allgeier A, Lacombe D, Cairncross JG, Eisenhauer E and Mirimanoff RO; European Organisation for Research and Treatment of Cancer Brain Tumor and Radiotherapy Groups; National Cancer Institute of Canada Clinical Trials Group. Radiotherapy plus concomitant and adjuvant temozolomide for glioblastoma. N Engl J Med 2005; 352: 987-996.

[9] Cao Y, Tsien CI, Shen Z, Tatro DS, Ten Haken R, Kessler ML, Chenevert TL and Lawrence TS. Use of magnetic resonance imaging to assess blood-brain/blood-glioma barrier opening during conformal radiotherapy. J Clin Oncol 2005; 23: 4127-4136.

[10] Huang WJ, Chen WW and Zhang X. Glioblastoma multiforme: effect of hypoxia and hypoxia inducible factors on therapeutic approaches. Oncol Lett 2016; 12: 2283-2288.

[11] Joh DY, Sun L, Stangl M, Al Zaki A, Murty S, Santoiemma PP, Davis JJ, Baumann BC, Alonso-Basanta M, Bhang D, Kao GD, Tsourkas A and Dorsey JF. Selective targeting of brain tumors with gold nanoparticle-induced radiosensitization. PLoS One 2013; 8: e62425.

[12] Clavreul A, Pourbaghi-Masouleh M, Roger E and Menei P. Nanocarriers and nonviral methods for delivering antiangiogenic factors for glioblastoma therapy: the story so far. Int J Nanomedicine 2019; 14: 2497-2513.

[13] Alphandery E. Nano-therapies for glioblastoma treatment. Cancers (Basel) 2020; 12: 242.

[14] Zhang B, Sun X, Mei H, Wang Y, Liao Z, Chen J, Zhang Q, Hu Y, Pang Z and Jiang X. LDLR-mediated peptide-22-conjugated nanoparticles for dual-targeting therapy of brain glioma. Biomaterials 2013; 34: 9171-9182.

[15] Bertato MP, Oliveira CP, Wajchenberg BL, Lerario AC and Maranhao RC. Plasma kinetics of an LDL-like nanoemulsion and lipid transfer to HDL in subjects with glucose intolerance. Clinics (Sao Paulo) 2012; 67: 347-353.

[16] Kim HR, Gil S, Andrieux K, Nicolas V, Appel M, Chacun H, Desmaele D, Taran F, Georgin D and Couvreur P. Low-density lipoprotein receptor-mediated endocytosis of PEGylated nanoparticles in rat brain endothelial cells. Cell Mol Life Sci 2007; 64: 356-364.

[17] Jain A, Jain K, Kesharwani P and Jain NK. Low density lipoproteins mediated nanoplatforms

for cancer targeting. J Nanopart Res 2013; 15: 1888.
[18] Nikanjam M, Gibbs AR, Hunt CA, Budinger TF and Forte TM. Synthetic nano-LDL with paclitaxel oleate as a targeted drug delivery vehicle for glioblastoma multiforme. J Control Release 2007; 124: 163-171.
[19] Andre S, Larbanoix L, Verteneuil S, Stanicki D, Nonclercq D, Vander Elst L, Laurent S, Muller RN and Burtea C. Development of an LDL receptor-targeted peptide susceptible to facilitate the brain access of diagnostic or therapeutic agents. Biology (Basel) 2020; 9: 161.
[20] Wang S, Meng Y, Li C, Qian M and Huang R. Receptor-mediated drug delivery systems targeting to glioma. Nanomaterials (Basel) 2015; 6: 3.
[21] Alan Mitteer R, Wang Y, Shah J, Gordon S, Fager M, Butter PP, Jun Kim H, Guardiola-Salmeron C, Carabe-Fernandez A and Fan Y. Proton beam radiation induces DNA damage and cell apoptosis in glioma stem cells through reactive oxygen species. Sci Rep 2015; 5: 13961.
[22] Seo SJ, Jeon JK, Han SM and Kim JK. Reactive oxygen species-based measurement of the dependence of the coulomb nanoradiator effect on proton energy and atomic Z value. Int J Radiat Biol 2017; 93: 1239-1247.
[23] Seo SJ, Lee SH, Kim KH and Kim JK. Anti-Flt1 peptide and cyanine-conjugated gold nanoparticles for the concurrent antiangiogenic and endothelial cell proton treatment. J Biomed Mater Res B Appl Biomater 2019; 107: 1272-1283.
[24] Kundu K, Knight SF, Willett N, Lee S, Taylor WR and Murthy N. Hydrocyanines: a class of fluorescent sensors that can image reactive oxygen species in cell culture, tissue, and in vivo. Angew Chem Int Ed Engl 2009; 48: 299-303.
[25] Srinivasan B, Kolli AR, Esch MB, Abaci HE, Shuler ML and Hickman JJ. TEER measurement techniques for in vitro barrier model systems. J Lab Autom 2015; 20: 107-126.
[26] Gandhi N, Saiyed ZM, Napuri J, Samikkannu T, Reddy PV, Agudelo M, Khatavkar P, Saxena SK and Nair MP. Interactive role of human immunodeficiency virus type 1 (HIV-1) clade-specific Tat protein and cocaine in blood-brain barrier dysfunction: implications for HIV-1-associated neurocognitive disorder. J Neurovirol 2010; 16: 294-305.
[27] Krstulja M, Bonifacic D and Cvejanović S. Proliferation of endothelial cells in neoangiogenesis of human cortical glioblastoma. Cent Eur J Biol 2008; 3: 113-119.
[28] Soda Y, Marumoto T, Friedmann-Morvinski D, Soda M, Liu F, Michiue H, Pastorino S, Yang M, Hoffman RM, Kesari S and Verma IM. Transdifferentiation of glioblastoma cells into vascular endothelial cells. Proc Natl Acad Sci U S A 2011; 108: 4274-4280.
[29] Guyon J, Chapouly C, Andrique L, Bikfalvi A and Daubon T. The normal and brain tumor vasculature: morphological and functional characteristics and therapeutic targeting. Front Physiol 2021; 12: 622615.
[30] Folkins C, Shaked Y, Man S, Tang T, Lee CR, Zhu Z, Hoffman RM and Kerbel RS. Glioma tumor stem-like cells promote tumor angiogenesis and vasculogenesis via vascular endothelial growth factor and stromal-derived factor 1. Cancer Res 2009; 69: 7243-7251.
[31] Cheng L, Huang Z, Zhou W, Wu Q, Donnola S, Liu JK, Fang X, Sloan AE, Mao Y, Lathia JD, Min W, McLendon RE, Rich JN and Bao S. Glioblastoma stem cells generate vascular pericytes to support vessel function and tumor growth. Cell 2013; 153: 139-152.
[32] Kim JK, Seo JS and Jeon JG. Ion beam stimulation therapy with a nanoradiator as a site-specific prodrug. Front Phys 2020; 8: 270-278.
[33] Gonias SL and Campana WM. LDL receptor-related protein-1: a regulator of inflammation in atherosclerosis, cancer, and injury to the nervous system. Am J Pathol 2014; 184: 18-27.
[34] Gao S, Tian H, Xing Z, Zhang D, Guo Y, Guo Z, Zhu X and Chen X. A non-viral suicide gene delivery system traversing the blood brain barrier for non-invasive glioma targeting treatment. J Control Release 2016; 243: 357-369.

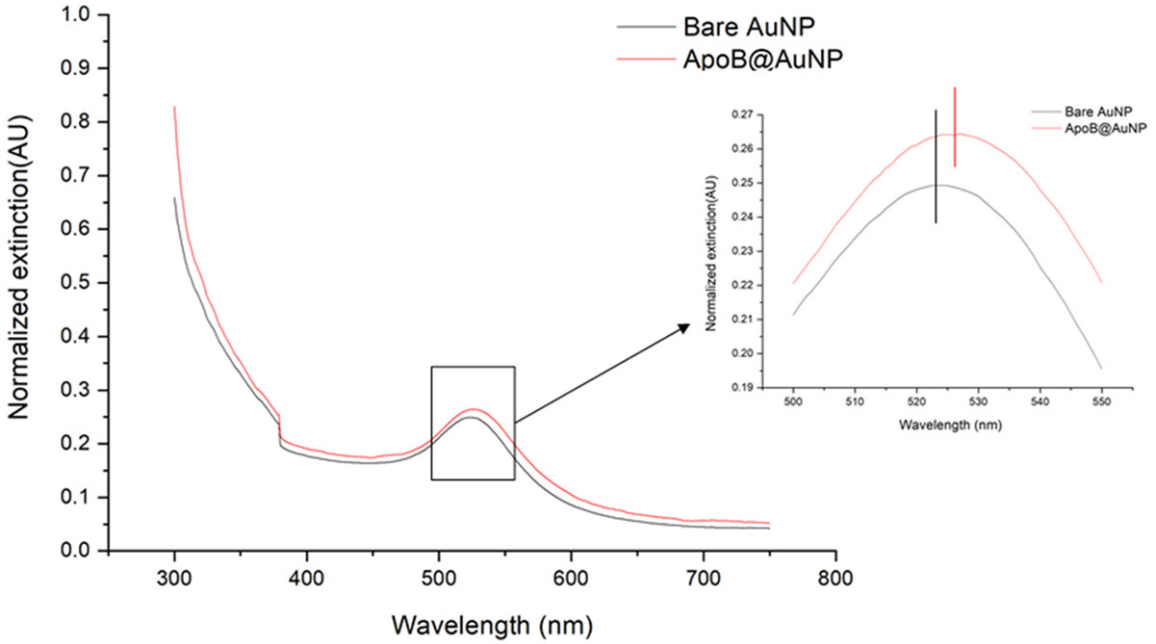

Supplementary Figure 1. Optical absorption of bare gold nanoparticle (Black) with a resonance at 523 nm and ApoB29mer-peptide conjugated gold nanoparticle (Red) showing red-shift resonance at 527 nm as clearly demonstrated in expanded window.

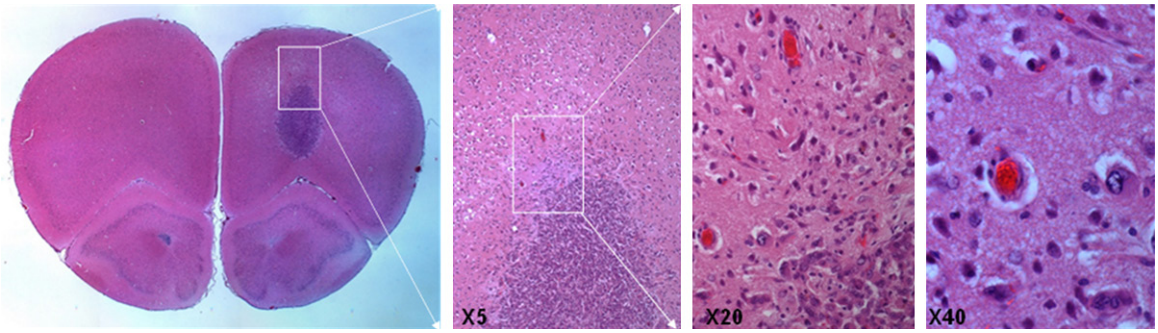

Supplementary Figure 2. Result of single proton treatment with a pristine transmission beam of 10 Gy entrance dose at 24 hours after intravenous injection of 150 mg AuNP/BW Kg in F98 rat glioma model showed absence of microvascular endothelial cell proliferation in TME and controlled tumor mass.